Repotrectinib (TPX-0005) Is a Next-Generation ROS1/TRK/ALK Inhibitor That Potently Inhibits ROS1/TRK/ALK Solvent-Front Mutations

Alexander Drilon[1], Sai-Hong Ignatius Ou[2], Byoung Chul Cho[3], Dong-Wan Kim[4], Jeeyun Lee[5], Jessica J. Lin[6], Viola W. Zhu[2], Myung-Ju Ahn[5], D. Ross Camidge[7], Judy Nguyen[1], Dayong Zhai[8], Wei Deng[8], Zhongdong Huang[8], Evan Rogers[8], Juliet Liu[8], Jeff Whitten[8], John K. Lim[8], Shanna Stopatschinskaja[8], David M. Hyman[1], Robert C. Doebele[7], J. Jean Cui[8], and Alice T. Shaw[6]

ABSTRACT

The use of tyrosine kinase inhibitors (TKI) with activity against ALK, ROS1, or TRKA–C can result in significant clinical benefit in patients with diverse tumors harboring *ALK, ROS1*, or *NTRK1–3* rearrangements; however, resistance invariably develops. The emergence of on-target kinase domain mutations represents a major mechanism of acquired resistance. Solvent-front substitutions such as ALK^{G1202R}, ROS1^{G2032R} or ROS1^{D2033N}, TRKA^{G595R}, and TRKC^{G623R} are among the most recalcitrant of these mechanisms. Repotrectinib (TPX-0005) is a rationally designed, low-molecular-weight, macrocyclic TKI that is selective and highly potent against ROS1, TRKA–C, and ALK. Importantly, repotrectinib exhibits activity against a variety of solvent-front substitutions *in vitro* and *in vivo*. As clinical proof of concept, in an ongoing first-in-human phase I/II trial, repotrectinib achieved confirmed responses in patients with *ROS1* or *NTRK3* fusion–positive cancers who had relapsed on earlier-generation TKIs due to ROS1 or TRKC solvent-front substitution-mediated resistance.

SIGNIFICANCE: Repotrectinib (TPX-0005), a next-generation ROS1, pan-TRK, and ALK TKI, overcomes resistance due to acquired solvent-front mutations involving *ROS1, NTRK1–3*, and *ALK*. Repotrectinib may represent an effective therapeutic option for patients with *ROS1-, NTRK1–3-, or ALK*-rearranged malignancies who have progressed on earlier-generation TKIs. *Cancer Discov; 8(10); 1227–36. ©2018 AACR.*

[1]Memorial Sloan Kettering Cancer Center, Weill Cornell Medical College, New York, New York. [2]Chao Family Comprehensive Cancer Center, University of California Irvine School of Medicine, Orange, California. [3]Yonsei Cancer Center, Severance Hospital, Yonsei University College of Medicine, Seoul, Republic of Korea. [4]Seoul National University Hospital, Seoul, Republic of Korea. [5]Samsung Medical Center, Sungkyunkwan University School of Medicine, Seoul, Republic of Korea. [6]Massachusetts General Hospital, Harvard Medical School, Boston, Massachusetts. [7]University of Colorado Denver, Anschutz Medical Campus, Aurora, Colorado. [8]TP Therapeutics Inc., San Diego, California.

Note: Supplementary data for this article are available at Cancer Discovery Online (http://cancerdiscovery.aacrjournals.org/).

A. Drilon and S.-H.I. Ou contributed equally to this article.

Corresponding Authors: Alice T. Shaw, Massachusetts General Hospital, 32 Fruit Street, Boston, MA 02114. Phone: 617-724-4000; Fax: 617-726-0453; E-mail: ashaw1@mgh.harvard.edu; and J. Jean Cui, TP Therapeutics, Inc., 10628 Science Center Drive, Ste. 225, San Diego, CA 92121. Phone: 858-926-5251; E-mail: jean.cui@tptherapeutics.com

doi: 10.1158/2159-8290.CD-18-0484

INTRODUCTION

The development and approval of earlier-generation tyrosine kinase inhibitors (TKI) for the treatment of *ALK*- and *ROS1*-rearranged non–small cell lung cancers (NSCLC) led to the appreciation of receptor tyrosine kinase fusions as targetable oncogenic driver alterations in a diverse group of solid malignancies (1–4). More recently, rearrangements involving *NTRK1, NTRK2*, and *NTRK3*, encoding TRKA, TRKB, and TRKC, respectively, have been identified as oncogenic drivers in a variety of different tumor types. *NTRK*-rearranged cancers are exquisitely sensitive to targeted therapies that inhibit TRK regardless of age and tumor origin (5, 6).

Despite the clinical activity of TKIs, resistance invariably develops. Moreover, particularly recalcitrant mechanisms of on-target resistance can emerge in fusion-positive tumors, especially after exposure to potent TKIs. The acquisition of mutations resulting in amino acid substitutions at the kinase solvent front represents an example of such a mechanism. These substitutions that occur secondary to solvent-front mutations (SFM) include ALK^{G1202R} in *ALK*-rearranged tumors, ROS1^{G2032R} and ROS1^{D2033N} in *ROS1*-rearranged tumors, and TRKA^{G595R} and TRKC^{G623R} in *NTRK1*- and *NTRK3*-rearranged tumors, respectively (7–17). In *ALK*-rearranged cancers, ALK^{G1202R} is commonly observed after treatment with more potent, earlier-generation agents and can occur in approximately a third of patients who relapse on second-generation ALK TKIs such as alectinib and ceritinib (10). Similarly, ROS1^{G2032R} can also emerge in about one third of patients after crizotinib failure, with an additional 5% of patients developing another solvent-front substitution, ROS1^{D2033N} (14, 15). Solvent-front substitutions were reported in *NTRK*-rearranged cancers after entrectinib treatment and mediated resistance in the majority (7 of 10 tested) of *NTRK*-rearranged cancers after larotrectinib treatment (5, 6).

In this report, we describe the preclinical activity of repotrectinib (TPX-0005), a rationally designed next-generation TKI developed to potently inhibit clinically recalcitrant solvent front substitutions involving ROS1, TRKA–C, and ALK, in addition to wild-type (WT) ROS1, TRKA–C, and ALK and other clinically relevant non–solvent front mutations. We also demonstrate proof-of-principle clinical activity in an ongoing phase I/II clinical trial investigating the safety and efficacy of repotrectinib (www.clinicaltrials.gov: NCT03093116).

RESULTS

Design and Structure

Many currently available ALK, ROS1, and TRKA–C inhibitors are ATP-competitive type I TKIs that have an ATP adenine-equivalent kinase hinge binder (Supplementary Fig. S1). These agents have an extra motif extending to the solvent area, which represents a shared liability in the setting of on-target resistance mediated by the acquisition of SFMs (Supplementary Figs. S2 and S3). Repotrectinib was designed to overcome clinical resistance mutations, especially SFMs (Supplementary Figs. S4–S6 and Supplementary Table S1). Structurally, the drug is a rigid, three-dimensional macrocycle that precisely anchors the molecule in the adenine binding site with a bioactive binding conformation predefined to avoid the entropy penalty after binding. Furthermore, repotrectinib is smaller in size compared with currently available ROS1, TRKA–C, and ALK inhibitors in the clinic, with favorable central nervous system (CNS) drug-like properties for human brain penetration (Supplementary Table S2A and S2B). This novel design was aimed to target both WT and SFM kinases (Supplementary Table S3) as well as other resistance mutations identified in the clinic as demonstrated by its preclinical activity against various *ALK*-mutant kinases (Supplementary Table S4). Structural modeling predicts that repotrectinib can accommodate the bulky, positively charged arginine side chain in the solvent front without any steric clashes. These solvent-front substitutions include ROS1^{G2032R} and ROS1^{D2033N}, TRKA^{G595R}, TRKB^{G639R}, TRKC^{G623R}, and ALK^{G1202R} (Fig. 1).

Enzyme and Cell-Based Activity

Repotrectinib inhibited the kinase activity of WT ROS1, TRKA–C, and ALK, and their SFMs with IC_{50} values in the range of 0.071 to 4.46 nmol/L (Supplementary Table S3). Based on the high potency against ROS1/TRKA–C/ALK, the kinase selectivity of repotrectinib was screened at 100 nmol/L against 395 distinct kinases. Screening hits were further evaluated for kinase inhibition IC_{50} values (Supplementary Table S5). Repotrectinib showed high potency against ROS1 and TRKA–C with approximately 15-fold selectivity over ALK. In addition, repotrectinib inhibited JAK2 and multiple SRC family members in biochemical assays (Fig. 2A).

Because each kinase has a distinct binding affinity (K_m) with ATP and a unique conformation in cells, kinase selectivity was further evaluated at the cellular level. Repotrectinib inhibited the phosphorylation of ROS1 and TRKA with IC_{50}s of <1 nmol/L in NIH3T3 CD74–ROS1 and KM12 cells, and ALK with IC_{50} of <3 nmol/L in Karpas-299 cells (Supplementary Fig. S7). Repotrectinib inhibited JAK2 substrate STAT5 phosphorylation (IC_{50} 158 nmol/L) in SET2 cells, and SRC phosphorylation (IC_{50} 89 nmol/L) in H2228 cells (Supplementary Fig. S7). Overall, repotrectinib demonstrated high selectivity for ROS1, TRKA–C, and ALK in cell-based phosphorylation assays.

Ba/F3 cells were engineered to express WT fusion proteins [CD74–ROS1, LMNA–TRKA, ETV6–TRKB, ETV6–TRKC, and EML4–ALK variant 1 (v1)] or corresponding solvent-front substitutions (ROS1^{G2032R}, ROS1^{D2033N}, TRKA^{G595R}, TRKB^{G639R}, TRKC^{G623R}, TRKC^{G623E}, and ALK^{G1202R}). In models harboring WT ROS1 fusion proteins, repotrectinib and lorlatinib were more potent (IC_{50} values <0.2 and 0.2 nmol/L) compared with crizotinib, entrectinib, ceritinib, brigatinib, cabozantinib, and ensartinib (Fig. 2B). As predicted, ROS1^{G2032R} and ROS1^{D2033N} rendered resistance to crizotinib, entrectinib, ceritinib, brigatinib, and ensartinib. Although lorlatinib retained activity against these mutations in preclinical studies (7), repotrectinib and cabozantinib were substantially more potent than lorlatinib against ROS1^{G2032R}, with IC_{50} values of 3.3 and 11 nmol/L, respectively, compared with an IC_{50} of 160.7 nmol/L for lorlatinib. For ROS1^{D2033N}, repotrectinib was slightly less potent than cabozantinib (1.3 vs. 0.2 nmol/L), but more potent than lorlatinib (3.3 nmol/L; Supplementary Fig. S8A and Supplementary Table S6A).

In Ba/F3 models harboring WT TRKA–C fusion proteins, repotrectinib was more potent (IC_{50} <0.2 nmol/L) compared with larotrectinib and entrectinib (Fig. 2C). The drug retained potent activity against TRKA^{G595R} (IC_{50} 0.4 nmol/L),

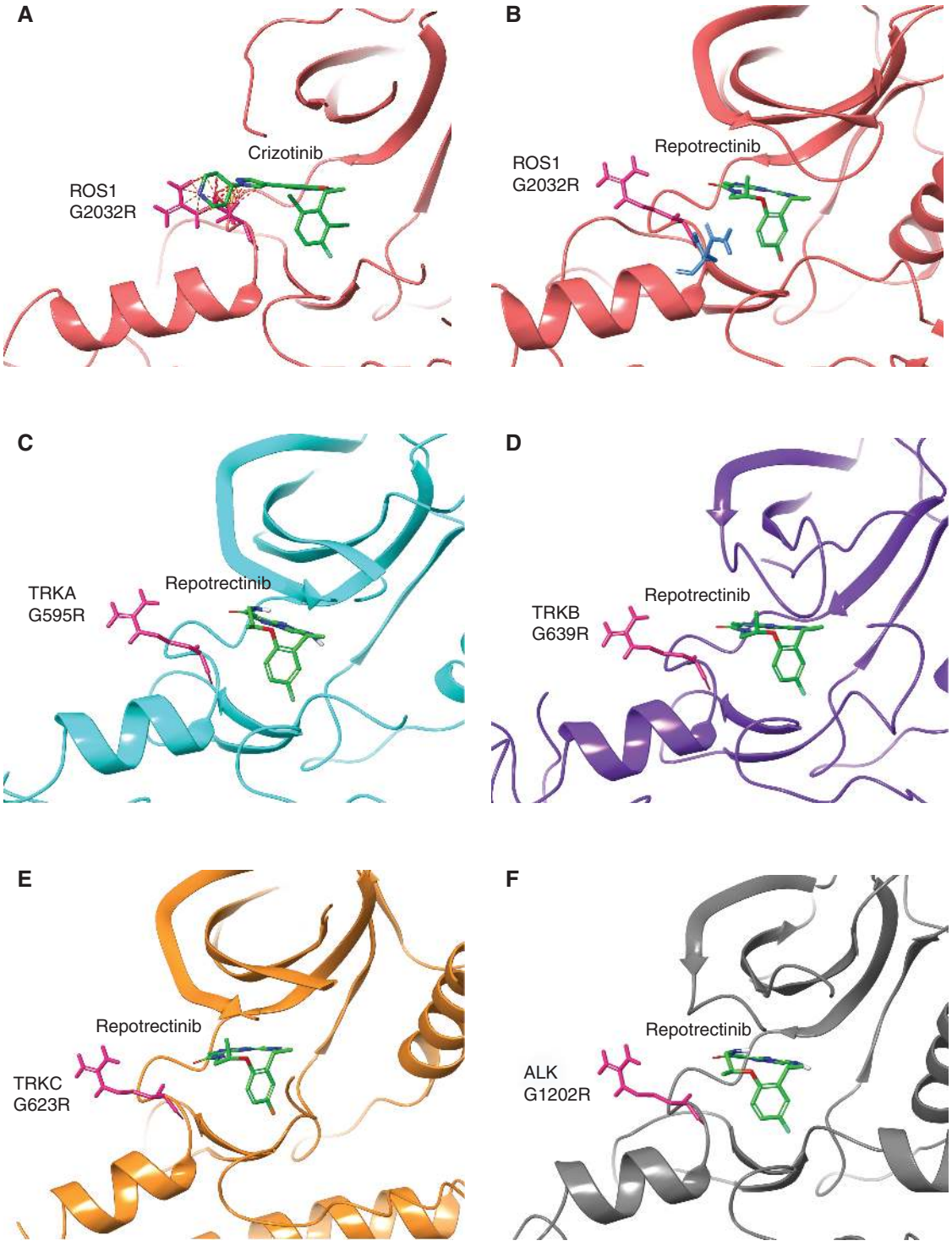

Figure 1. Binding of repotrectinib to ROS1, TRKA–C, and ALK kinases with solvent-front substitutions. Crizotinib has a basic piperidine group that extends to the solvent-front area, thus clashing with ROS1 solvent-front substitution. ROS1, TRKA–C, and ALK solvent-front substitutions (located at the C-terminus of the ATP adenine binding hinge) mediate resistance to therapy. Similar to crizotinib, other currently available ROS1, TRKA–C, and ALK inhibitors carry an extra motif that likewise extends to the solvent area that sterically clashes with solvent-front substitutions. In order to avoid this steric inteference, repotrectinib was designed to be much smaller in size (MW 355.37) than the currently available ROS1, TRKA–C, and ALK inhibitors. As shown here, repotrectinib (green) has a rigid three-dimensional macrocyclic structure that precisely anchors the molecule completely inside the ATP adenosine binding site of the cocrystal structure of ROS1, TRKA–C, and ALK with a predefined bioactive binding conformation. Structural modeling studies indicate that steric clashes do not occur between repotrectinib and SFMs involving ROS1, TRKA–C, and ALK.

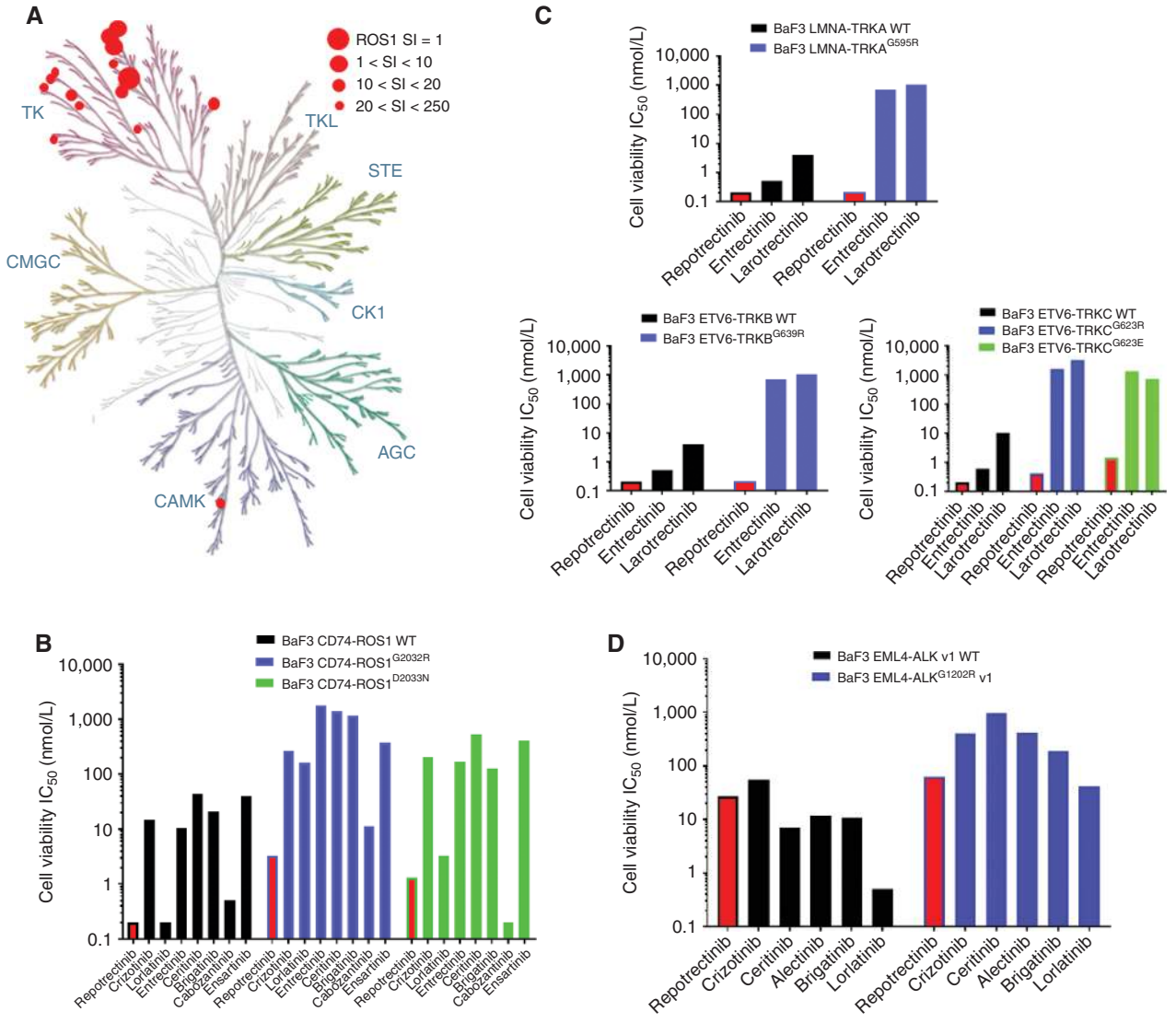

Figure 2. Selectivity and *in vitro* antiproliferative activity of repotrectinib. **A,** The selectivity of repotrectinib for 395 distinct kinases is shown in this kinome tree. The selectivity index (SI) is defined as the kinase IC_{50} value divided by the ROS1 IC_{50} value (0.071 nmol/L) and is depicted by the size of the circles: the largest circle is ROS1 with an SI value of 1, followed by TRKA, TRKB, and TRKC with SI values between 1 and 10, followed by ALK, JAK2, and FYN with SI values between 10 and 20. Kinases with SI values greater than 20 but less than 250 are LYN, YES1, FGR, TXK, ARK5, SRC, DDR1, and FAK. **B,** Antiproliferation activity of repotrectinib, crizotinib, lorlatinib, entrectinib, ceritinib, brigatinib, cabozantinib, and ensartinib against Ba/F3 cells engineered with CD74–ROS1 WT, CD74–ROS1^{G2032R}, or CD74–ROS1^{D2033N} fusion proteins, respectively. **C,** Antiproliferation activity of repotrectinib, entrectinib, and larotrectinib against Ba/F3 cells engineered with LMNA–TRKA WT, LMNA–TRKA^{G595R}, ETV6–TRKB WT, ETV6–TRKB^{G639R}, ETV6–TRKC WT, ETV6–TRKC^{G623R}, or ETV6–TRKC^{G623E} fusion proteins, respectively. **D,** Antiproliferation activity of repotrectinib, crizotinib, ceritinib, alectinib, brigatinib, and lorlatinib against Ba/F3 cells engineered with EML4–ALK v1 WT or EML4–ALK^{G1202R} v1 fusion proteins.

TRKB^{G639R} (IC_{50} 0.6 nmol/L), TRKC^{G623R} (IC_{50} 0.2 nmol/L), and TRKC^{G623E} (IC_{50} 1.4 nmol/L), whereas these substitutions rendered resistance to larotrectinib and entrectinib. In addition, repotrectinib was 46- and 62-fold more potent than entrectinib and larotrectinib, respectively, at inhibiting KM12 cell proliferation (IC_{50} 0.2 nmol/L; Supplementary Fig. S8B; Supplementary Table S6B).

Similarly, in Ba/F3 models harboring WT EML4–ALK variant 1, repotrectinib (IC_{50} 27 nmol/L) was more potent than crizotinib, had comparable activity with alectinib, ceritinib, and brigatinib, and was less potent than lorlatinib (Fig. 2D); however, the drug retained potent activity against ALK^{G1202R} (IC_{50} 63.6 nmol/L), comparable with that seen with lorlatinib (IC_{50} 41.5 nmol/L). In addition, repotrectinib inhibited Karpas-299 cell proliferation (IC_{50} 23.7 nmol/L) with a similar potency as alectinib (Supplementary Fig. S8C; Supplementary Table S6C).

Overall, repotrectinib was a potent ROS1/TRK/ALK inhibitor in both enzymatic and cellular assays, and selectively cytotoxic to engineered cell lines with *ROS1, NTRK*, or *ALK* rearrangements, while having IC_{50} >1,000 nmol/L for parental Ba/F3 cells (Supplementary Table S6C) and cell lines with other oncogene drivers (Supplementary Table S6D).

In Vivo Activity

The *in vivo* activity of repotrectinib was tested against representative SFMs, ROS1^{G2032R}, TRKA^{G595R}, and ALK^{G1202R}, using mouse xenograft models. In SCID/Beige mice bearing Ba/F3 CD74–ROS1 WT or CD74–ROS1^{G2032R} xenograft tumors, the twice-daily (b.i.d.) dosing with 15 or 75 mg/kg/dose of crystalline repotrectinib resulted in a free C_{trough} of 2.2 and 13.3 nmol/L, and tumor growth inhibition (TGI) of 197% and 200% against CD74–ROS1 WT tumors (Fig. 3A) and 99% and 200% against CD74–ROS1^{G2032R} tumors (Fig. 3B), respectively, without body-weight loss (Supplementary Fig. S9A). A free C_{trough} of 13.3 nmol/L led to complete tumor regression in ROS1 WT and G2032R tumor models. The mean trough plasma concentration is summarized in Supplementary Table S7.

In athymic nude mice bearing NIH3T3 LMNA–TRKA WT xenograft tumors, a micronized crystalline formulation of repotrectinib was used for b.i.d. dosing at 3 or 15 mg/kg/dose, leading to a free C_{trough} of 3.5 and 22.7 nmol/L, and TGIs of 100% and 128%, respectively (Fig. 3C), whereas entrectinib achieved a TGI of 98% at 15 mg/kg b.i.d. dosing. The treatment with micronized crystalline repotrectinib at 3, 15, or 60 mg/kg/dose b.i.d. resulted in a free C_{trough} of 3.5, 22.7, and 173.5 nmol/L, leading to TGIs of 56%, 97%, and 123%, respectively, in the TRKA^{G595R} tumor model (Fig. 3D) without body-weight loss (Supplementary Fig. S9B), whereas entrectinib had 78% TGI at 60 mg/kg b.i.d. A free C_{trough} of 22.7 nmol/L was required to achieve 97% TGI in the NIH3T3 LMNA–TRKA^{G595R} tumor model. The mean trough plasma concentration is summarized in Supplementary Table S7.

The activity of repotrectinib was investigated in SCID/Beige mice bearing Ba/F3 EML4–ALK v1 WT or EML4–ALK v1 G1202R xenograft tumors. The b.i.d. dosing with 15 or 75 mg/kg of the crystalline repotrectinib resulted in TGIs of 75% and 154% against EML4–ALK v1 WT tumors (Fig. 3E), and 56% and 99% against EML4–ALK v1 G1202R tumors (Fig. 3F), respectively, without body-weight loss (Supplementary Fig. S9C). Therefore, a free C_{trough} of 13.3 nmol/L was required

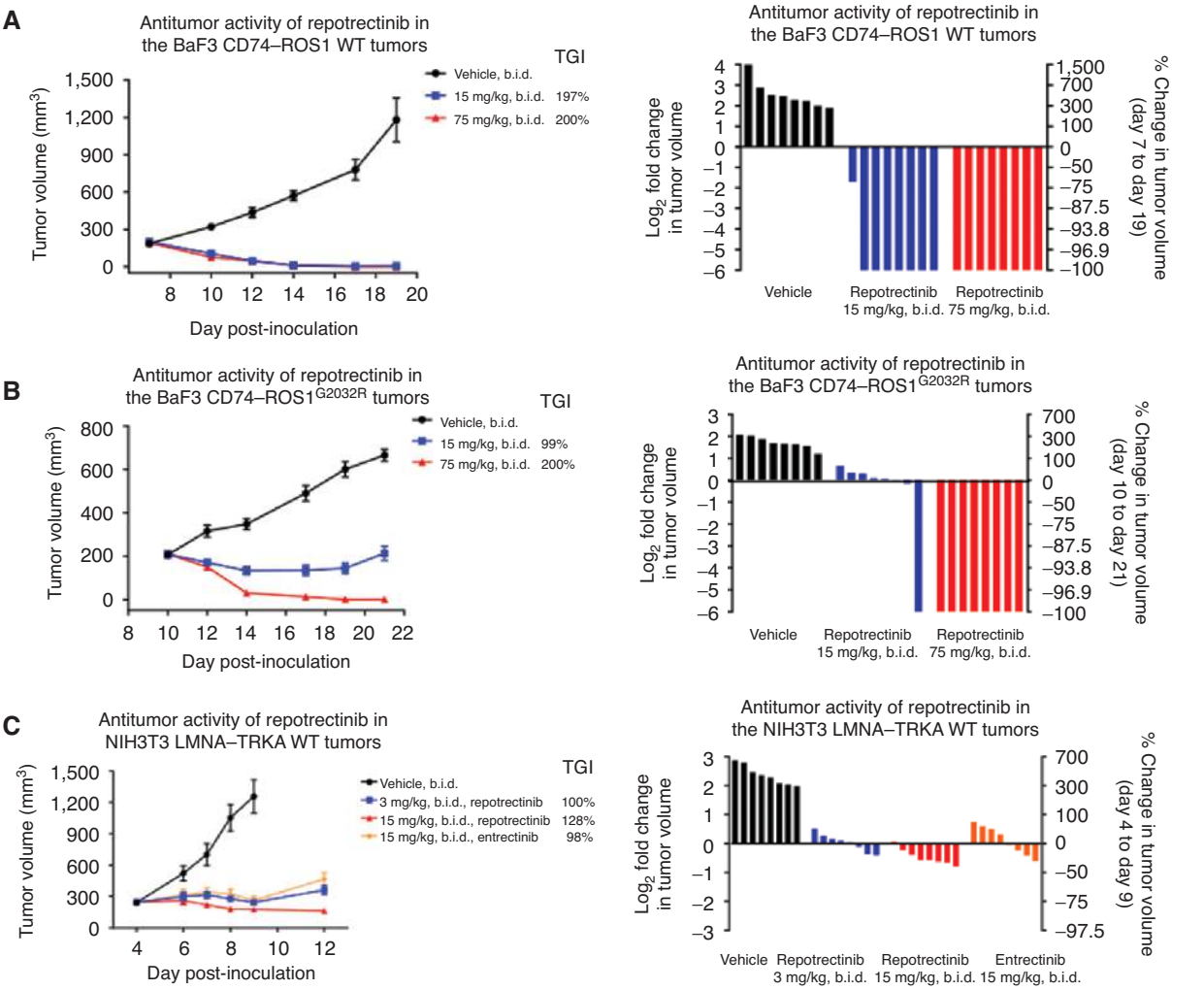

Figure 3. *In vivo* antitumor activity of repotrectinib. The antitumor activity of repotrectinib in the following fusion-positive xenograft models, several of which harbor SFMs, is shown: **A,** Ba/F3 CD74–ROS1 WT in SCID/Beige mice; **B,** Ba/F3 CD74–ROS1^{G2032R} in SCID/Beige mice; **C,** NIH3T3 LMNA–TRKA WT in athymic nude mice; (*continued on next page*)

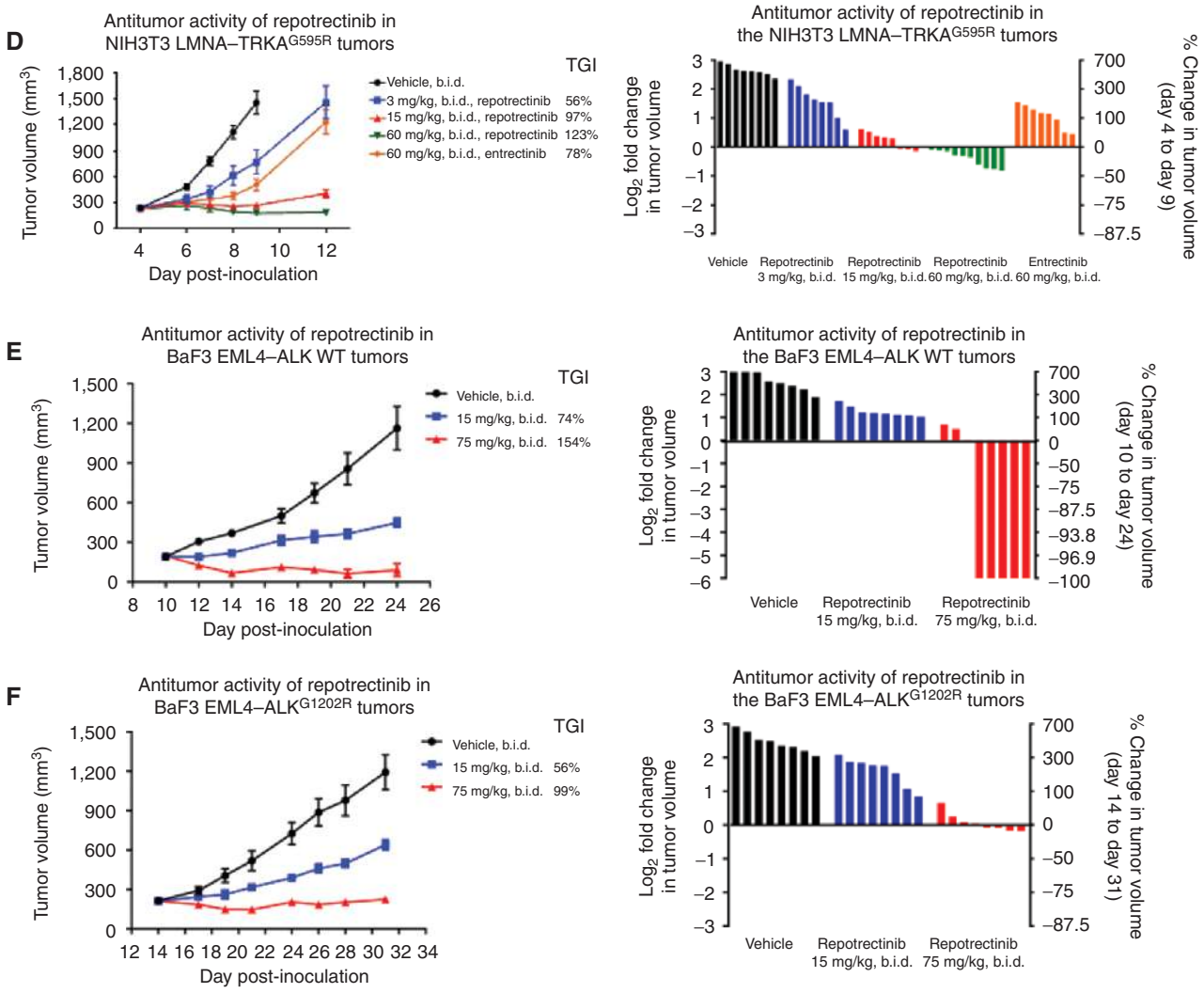

Figure 3. ***(Continued)*** **D,** NIH3T3 LMNA–TRKA^{G595R} in athymic nude mice; **E,** Ba/F3 EML4–ALK v1 WT in SCID/Beige mice; **F,** Ba/F3 EML4–ALK^{G1202R} v1 in SCID/Beige mice. The comparative activity of entrectinib is included in **C** and **D**. Graphs of tumor volume changes in response to treatment with vehicle and various doses of repotrectinib or entrectinib are shown on the left. Each corresponding waterfall plot on the right represents the degree of xenograft response in one mouse. Tumor regression or stabilization was observed with repotrectinib in all models, including resistant models harboring SFMs.

to achieve 99% TGI in the Ba/F3 EML4–ALK v1 G1202R tumor model. The mean trough plasma concentration is summarized in Supplementary Table S7.

Proof-of-Concept Clinical Activity

Repotrectinib is being investigated in an ongoing first-in-human dose-escalation phase I/II clinical trial (NCT03093116) in patients with advanced *ALK*-, *ROS1*-, or *NTRK1–3*-rearranged cancers.

ETV6–NTRK3^{G623E+} Mammary Analogue Secretory Carcinoma

A 44-year-old man presented in October of 2012 with a right parotid mass. He underwent a right parotidectomy and a mammary analogue secretory carcinoma (MASC) was identified. His history was thereafter marked by recurrent local disease requiring two subsequent resections and chemoradiation. In 2015, he developed recurrent local disease in addition to metastatic disease involving the lungs. Genomic profiling later revealed an *ETV6–NTRK3* rearrangement. Crizotinib was initiated with a best response of progressive disease. The patient was then enrolled onto a clinical trial of entrectinib that he received for 6 months with partial response, followed by doxorubicin on progression of disease, and later entrectinib and trametinib, which the patient received for 2 months with progressive disease. He was then enrolled onto the phase I trial of repotrectinib (40 mg once daily). A pretreatment biopsy revealed persistence of an in-frame *ETV6–NTRK3* rearrangement containing the kinase domain of *NTRK3* and an *NTRK3*^{G623E} mutation that was not present on a pre-entrectinib biopsy. A rapid and dramatic response to repotrectinib was achieved within the first few days of administration, noted as substantial shrinkage of externally visible disease involving the right mandibular area (Fig. 4A and B). Plasma exposures indicated that the C_{trough}

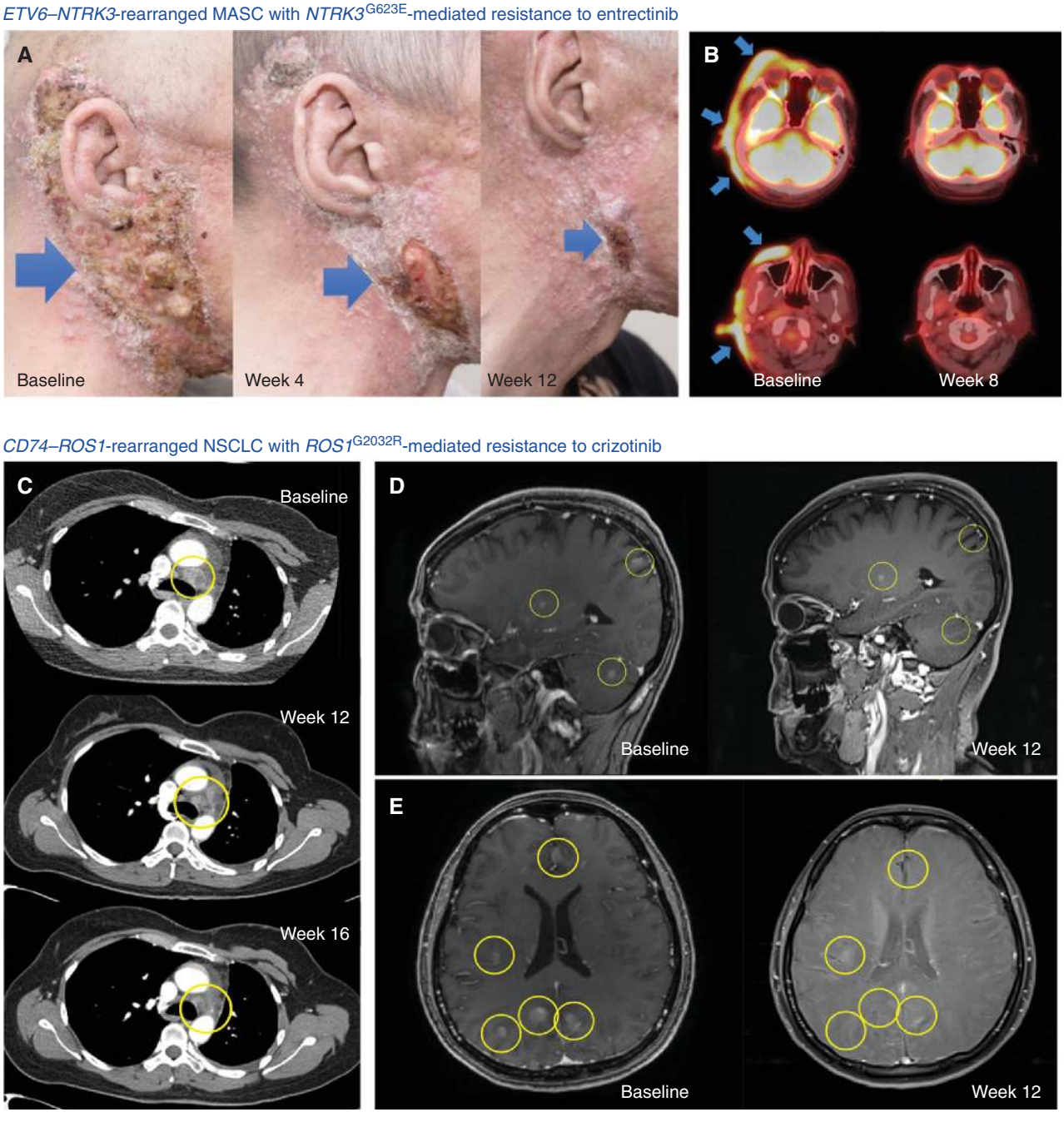

Figure 4. Response to repotrectinib in solvent-front substitution–containing cancers. **A,** A brisk and dramatic response to repotrectinib was observed in externally visible tumors from a patient with an *ETV6–NTRK3*–rearranged mammary analogue secretory carcinoma (MASC) harboring an *NTRK3*^{G623E} solvent-front mutation acquired after prior treatment with entrectinib. **B,** Combined computed and positron emission tomography images show a concurrent metabolic and radiologic response (regression of dermal and subcutaneous metastases) to therapy that was subsequently confirmed with follow-up imaging. The patient remains on repotrectinib at more than 17 months. **C,** Similarly, a confirmed radiologic response to therapy was achieved in a patient with a *CD74–ROS1*-rearranged NSCLC that acquired a *ROS1*^{G2032R} solvent-front mutation after prior treatment with crizotinib. Regression of a subcarinal node is shown. **D** and **E,** The intracranial activity of repotrectinib is shown, with magnetic resonance imaging demonstrating regression or disappearance of multiple previously untreated supratentorial and infratentorial brain metastases. The patient remains on repotrectinib at more than 12 months since treatment initiation. Yellow circles indicate areas of metastatic disease.

(144 nmol/L) was above the IC_{90} (80 nmol/L) needed to inhibit $TRKC^{G623E}$ Ba/F3 cell growth (Supplementary Fig. S10A). Radiologic imaging after 8 weeks of therapy revealed a partial response (PR) with shrinkage of multiple areas of disease involving the right cheek, cervical lymph nodes, chest wall nodules, and pulmonary and pleural nodules, followed by a confirmed PR with 82% tumor shrinkage by RECIST v1.1. The patient's cancer started to progress slowly after 6 months of treatment and his repotrectinib dose was gradually escalated to 160 mg b.i.d. as permitted by the protocol; this resulted in the reestablishment of disease control. He remains on therapy at 17+ months at the time of manuscript submission with no dose-limiting toxicities and only mild grade 1 peripheral sensory neuropathy. The clinical outcome is consistent with the cell-based inhibitory assay (Fig. 2C) and the mice xenograft study (Supplementary Fig. S10B).

CD74–$ROS1^{G2032R+}$ NSCLC

A 41-year-old Asian female never-smoker presented with stage IV NSCLC with a large pleural effusion, pleural-based nodules, and multiple enlarged mediastinal and supraclavicular lymph nodes. Pleural effusion cytology and supraclavicular lymph node fine-needle aspirate cytology both revealed adenocarcinoma. Molecular profiling identified a *CD74–ROS1* rearrangement. An MRI of the brain was negative for intracranial metastasis at the time of diagnosis. She received one cycle of carboplatin/pemetrexed/bevacizumab while awaiting insurance authorization for crizotinib. She started on crizotinib in June 2016 and had a durable response for 12 months, at which time imaging showed increasing mediastinal lymphadenopathy (Fig. 4C). A repeat biopsy and comprehensive genomic profiling at Foundation Medicine revealed *CD74–ROS1* and a $ROS1^{G2032R}$ SFM. The patient subsequently enrolled on the phase I repotrectinib trial and received repotrectinib at 160 mg once daily. Pre-repotrectinib brain imaging revealed multiple, clinically asymptomatic supratentorial and infratentorial brain metastases (Fig. 4D). She tolerated repotrectinib treatment well with mild grade 1 ataxia, paresthesias, and nausea early in her course that resolved with supportive care, and ongoing mild grade 1 perioral numbness and dysgeusia. A confirmed PR (−36.6%) by RECIST v1.1 was achieved with a duration of response of 7.4 months. Of note, this patient also responded to repotrectinib in the CNS for 9 months with subsequent CNS-only progression controlled by whole-brain radiation (WBRT) with continuation of repotrectinib during WBRT without any adverse events. After WBRT, the patient continued on repotrectinib beyond progression as permitted by protocol with continual extracranial partial response as of August 2018 (Fig. 4D and E). The patient had a new CNS lesion at Cycle 10 and remains on repotrectinib treatment at 12+ months after local brain radiation therapy as permitted by the protocol. Pharmacokinetic analyses revealed that the C_{trough} (425 nmol/L) was above the IC_{90} (100 nmol/L) needed to inhibit $ROS1^{G2032R}$ Ba/F3 cell proliferation (Supplementary Fig. S10C).

DISCUSSION

In cancers driven by gene fusions, sequential TKI therapy has emerged as a paradigm for maintaining disease control in the face of continued dependence on the fusion oncoprotein. The emergence of SFMs during the course of treatment, especially following more potent TKIs, represents a significant therapeutic challenge (9–19). Repotrectinib, by targeting the center of the ATP binding site with a small, three-dimensional macrocyclic structure, effectively circumvents steric hindrance from solvent-front substitutions. Consistent with this, in multiple preclinical models, repotrectinib demonstrated potent antiproliferative activity against WT fusion proteins involving ROS1, TRKA, TRKB, TRKC, and ALK, and their corresponding SFMs in cellular inhibitory assays and xenograft models.

For ROS1, both ceritinib (19) and entrectinib (20) have demonstrated clinical activity in crizotinib-naïve $ROS1^{+}$ NSCLC patients. Additionally, cabozantinib has demonstrated activity against ROS1 SFMs (14, 21). Lorlatinib is a next-generation ALK/ROS1 inhibitor with potent inhibitory activity against WT ROS1. In an ongoing phase I/II study, lorlatinib demonstrated variable clinical activity in patients with crizotinib-refractory $ROS1^{+}$ NSCLC (22, 23). Lorlatinib can inhibit the ROS1 gatekeeper substitution L2026M *in vitro* but is not as potent against the solvent-front substitution $ROS1^{G2032R}$ (7). Indeed, repotrectinib exhibits more potent inhibitory activity against WT ROS1 and SFMs than all other ROS1 TKIs with the exception of cabozantinib against D2033N [0.2 nmol/L (cabozantinib) vs. 1.3 nmol/L (repotrectinib)]. Overall, repotrectinib exhibited potent antiproliferative activity in Ba/F3 cells transduced with the oncogenic driver CD74–ROS1 and effectively inhibited $ROS1^{G2032R}$ (3.3 nmol/L) and D2033N (1.3 nmol/L; Supplementary Table S6A). Consistent with these results, repotrectinib induced a durable and ongoing response in a crizotinib-refractory patient with a *ROS1*-rearranged tumor harboring $ROS1^{G2032R}$.

Currently, no targeted therapy is approved for *NTRK*-rearranged cancers. The first-generation agent larotrectinib demonstrated marked antitumor activity in patients with *NTRK*-rearranged cancers (6). Similarly, entrectinib is active in patients with *NTRK*-rearranged cancer (5). On-target resistance frequently emerges with the use of either agent, including the acquisition of SFMs in 7 of 10 patients treated with larotrectinib (6), although a larger data set is required to determine the true frequency of on-target resistance in this context. Repotrectinib is highly potent against TRKA–C solvent-front substitutions preclinically, and a dramatic response to therapy was observed in a patient with an *NTRK3* fusion–positive tumor harboring an SFM. It remains to be determined whether there are any differences in clinical activity between repotrectinib and LOXO-195, another next-generation TRK inhibitor currently in clinical development (24).

Although repotrectinib is 15-fold less potent against ALK than ROS1 in enzymatic assays, repotrectinib has superior ALK inhibitory activity compared with the first-generation ALK inhibitor crizotinib and compares favorably in its ALK^{G1202R} inhibitory activity against currently approved second-generation ALK inhibitors (ceritinib, alectinib, and brigatinib). The current phase I trial will investigate the clinical activity of repotrectinib in *ALK*-rearranged malignancies.

Finally, CNS progression is a significant clinical challenge in oncogene-driven lung cancers, including *ALK*- and *ROS1*-rearranged NSCLC. The available next-generation ALK inhibitors have significantly improved CNS activity over crizotinib (25). Although the incidence of CNS metastasis may be lower

in patients with *ROS1* fusion–positive compared with *ALK* fusion–positive lung cancer, the incidence of CNS metastases increases with time on treatment (15). As shown in the preliminary clinical data presented in this report, repotrectinib has demonstrated proof-of-concept CNS activity against untreated brain metastases in a patient with a crizotinib-refractory, *ROS1* fusion–positive lung cancer.

In summary, this is the first report on the design and preclinical evaluation of the novel next-generation ROS1/TRK/ALK TKI repotrectinib. Repotrectinib was specifically designed to overcome refractory SFMs which commonly emerge in patients with *ROS1/NTRK/ALK*-rearranged malignancies who have relapsed on currently available TKIs. In an ongoing first-in-human dose-escalation trial, repotrectinib demonstrated antitumor activity in patients with *ROS1*- or *NTRK3*-rearranged tumors that harbor resistant SFMs. Although safety, dosing, and clinical efficacy are still being established, these findings suggest that repotrectinib could represent an effective treatment option for *ROS1/NTRK*-rearranged malignancies, including those harboring resistant SFMs. The clinical application of repotrectinib for TKI-refractory, *ALK* fusion–positive patients needs to be further defined in the ongoing trial.

METHODS

Preclinical Studies

Structural Modeling. Structural modeling of ALK, ROS1, and TRK solvent-front mutants in complex with repotrectinib (TPX-0005) was carried out with X-ray cocrystal structures of ALK (PDB 4CLJ), ROS1 (PDB 3ZBF and 4UXL), TRKA (PDB 4AOJ), TRKB (PDB 4AT3), and TRKC (PDB 4YMJ) using Schrodinger Maestro software (Supplementary Information).

Enzyme Assays. The enzymatic kinase inhibitory activities of repotrectinib were evaluated at Reaction Biology Corporation using the radiolabeled *HotSpot* kinase assay platform, and kinase selectivity was first evaluated using the KINOME*scan* site-directed competition binding assay against 456 human kinases at DiscoeRx. See Supplementary Information for detailed information.

Cell Lines and Assays. Human lung cancer cell line NCI-H2228 was obtained from the ATCC (2014). Cell lines NIH3T3 and Ba/F3 were purchased from DSMZ (2015, German Collection of Microorganisms and Cell Culture). Karpas-299 cell line was purchased and licensed from Sigma (2015). KM12 cell line was obtained from NCI (2015, Frederick Cancer DCTD Tumor Cell Repository). NCI-H2228, Karpas-299, and KM12 cells were authenticated by confirmation of the presence of each fusion (EML4–ALK, NPM–ALK, or TPM3–TRKA). NIH3T3 and Ba/F3 cells were not authenticated. Cell lines were confirmed to be *Mycoplasma*-free (Biomiga) and were used between 3 and 10 passages. The genes of EML4–ALK (variant 1), CD74–ROS1, LMNA–TRKA, ETV6–TRKB, ETV6–TRKC, and the solvent-front mutant genes of EML4–ALK^{G1202R}, CD74–ROS1^{G2032R}, CD74–ROS1^{G2033N}, LMNA–TRKA^{G595R}, ETV6–TRKB^{G639R}, ETV6–TRKC^{G623R}, and ETV6–TRKC^{G623E} were synthesized at GenScript and cloned into pCDH-CMV-MCS-EF1-Puro plasmid (System Biosciences, Inc.). The corresponding Ba/F3 and NIH3T3 stable cells were generated by transducing Ba/F3 cells and NIH3T3 cells with lentivirus containing the desired fusion gene or mutant. Please refer to Supplementary Information for detailed procedures.

For cellular phosphorylation assays, half a million cells per well were seeded in 24-well plate for 24 hours, and then treated with compounds for 4 hours. For cell proliferation assays, 2,000 cells per well were seeded in 384-well white plate for 24 hours, and then treated with compounds for 72 hours. Cell proliferation was measured using CellTiter-Glo luciferase-based ATP detection assay (Promega) following the manufacturer's protocol. Please refer to Supplementary Information for detailed procedures.

In Vivo *Xenograft Studies.* All animal studies were conducted in accordance with the guidelines as published in the Guide for the Care and Use of Laboratory Animals. Mice were maintained and used in accordance with the animal protocol EB15-013 (approved by Explora BioLabs' Institutional Animal Care and Use Committee). Five million cells in 100 μL serum-free medium supplemented with 50% Matrigel (Corning, Inc.) were implanted subcutaneously in the right flank region of the mouse. Mice were randomized by tumor size into treatment groups when tumor volume reached about 100 to 200 mm^3 and repotrectinib was administered orally (b.i.d.) at determined dosage. Tumor size and body weight were measured on designated days. Please refer to Supplementary Information for the detailed information.

Treatment Plan Design and Conduct

Repotrectinib is being investigated in a first-in-human dose-escalation study (NCT-03093116). The study has been conducted in accordance with recognized ethical guidelines such as the Declaration of Helsinki. The protocol has been approved by the institutional review boards at each participating site. Written informed consent was obtained from all the patients before screening. Details of eligibility criteria are listed at www.clinicaltrials.gov.

Disclosure of Potential Conflicts of Interest

A. Drilon has received honoraria from the speakers bureaus of TP Therapeutics, Ignyta, Loxo Oncology, and Ono. S.-H.I. Ou has received honoraria from the speakers bureaus of Roche/Genentech, AstraZeneca, and Takeda/ARIAD, has ownership interest (including stock, patents, etc.) in TP Therapeutics, is a member of the Scientific Advisory Board of TP Therapeutics, and served as a consultant for Pfizer, Roche Genentech, AstraZeneca, and Foundation Medicine. V.W. Zhu has received honoraria from the speakers bureaus of Roche-Foundation Medicine, Roche/Genentech, and Takeda, has ownership interest (including stock, patents, etc.) in TP Therapeutics, and is a consultant/advisory board member for TP Therapeutics. D.R. Camidge is a consultant/advisory board member for Takeda and Roche. D.M. Hyman reports receiving commercial research grants from Loxo Oncology, PUMA Biotechnology, and AstraZeneca and is a consultant/advisory board member for Pfizer, Genentech, Chugai, Atara, Boehringer Ingelheim, and CytomX. R.C. Doebele reports receiving a commercial research grant from Ignyta, has ownership interest (including stock, patents, etc.) in Rain Therapeutics, is a consultant/advisory board member for Takeda, AstraZeneca, and Ignyta, and has received other remuneration from Ignyta and Abbott Molecular. J.J. Cui has ownership interest (including stock, patents, etc.) in TP Therapeutics, Inc. A.T. Shaw is a consultant/advisory board member for member for TP Therapeutics, Pfizer, Blueprint Medicines, KSQ Therapeutics, Novartis, Roche/Genentech, LOXO, Ignyta, Takeda/Ariad, Foundation Medicine, Guardant, and Natera. No potential conflicts of interest were disclosed by the other authors.

Authors' Contributions

Conception and design: A. Drilon, S.-H.I. Ou, V.W. Zhu, D.R. Camidge, W. Deng, Z. Huang, J.J. Cui, A.T. Shaw

Development of methodology: A. Drilon, S.-H.I. Ou, V.W. Zhu, D. Zhai, Z. Huang, J.J. Cui

Acquisition of data (provided animals, acquired and managed patients, provided facilities, etc.): A. Drilon, S.-H.I. Ou, B.C. Cho, D.-W. Kim, J. Lee, J.J. Lin, V.W. Zhu, M.-J. Ahn, D.R. Camidge, J. Nguyen, D. Zhai, W. Deng, Z. Huang, E. Rogers, J. Liu, J. Whitten, J.K. Lim, S. Stopatschinskaja, D.M. Hyman, R.C. Doebele, A.T. Shaw

Analysis and interpretation of data (e.g., statistical analysis, biostatistics, computational analysis): A. Drilon, S.-H.I. Ou, B.C. Cho, D.-W. Kim, J.J. Lin, V.W. Zhu, D. Zhai, W. Deng, Z. Huang, J. Liu, J. Whitten, J.K. Lim, S. Stopatschinskaja, R.C. Doebele, J.J. Cui, A.T. Shaw
Writing, review, and/or revision of the manuscript: A. Drilon, S.-H.I. Ou, B.C. Cho, D.-W. Kim, J.J. Lin, V.W. Zhu, M.-J. Ahn, D.R. Camidge, D. Zhai, W. Deng, J.K. Lim, S. Stopatschinskaja, D.M. Hyman, R.C. Doebele, J.J. Cui, A.T. Shaw
Administrative, technical, or material support (i.e., reporting or organizing data, constructing databases): A. Drilon, J. Nguyen, D. Zhai, J.K. Lim, R.C. Doebele
Study supervision: A. Drilon, V.W. Zhu, M.-J. Ahn, J.K. Lim, R.C. Doebele, J.J. Cui, A.T. Shaw

Acknowledgments

Funding for this study was provided by TP Therapeutics, Inc.

Received May 2, 2018; revised June 27, 2018; accepted August 2, 2018; published first August 9, 2018.

REFERENCES

1. Kwak EL, Bang YJ, Camidge DR, Shaw AT, Solomon B, Maki RG, et al. Anaplastic lymphoma kinase inhibition in non-small-cell lung cancer. N Engl J Med 2010;363:1693–703.
2. Shaw AT, Ou SH, Bang YJ, Camidge DR, Solomon BJ, Salgia R, et al. Crizotinib in ROS1-rearranged non-small-cell lung cancer. N Engl J Med 2014;371:1963–71.
3. Shaw AT, Hsu PP, Awad MM, Engelman JA. Tyrosine kinase gene rearrangements in epithelial malignancies. Nat Rev Cancer 2013;13:772–87.
4. Schram AM, Chang MT, Jonsson P, Drilon A. Fusions in solid tumours: diagnostic strategies, targeted therapy, and acquired resistance. Nat Rev Clin Oncol 2017;14:735–48.
5. Drilon A, Siena S, Ou SI, Patel M, Ahn MJ, Lee J, et al. Safety and antitumor activity of the multitargeted pan-TRK, ROS1, and ALK inhibitor entrectinib: Combined results from two phase I trials (ALKA-372–001 and STARTRK-1). Cancer Discov 2017;7:400–9.
6. Drilon A, Laetsch TW, Kummar S, DuBois SG, Lassen UN, Demetri GD, et al. Efficacy of larotrectinib in TRK fusion-positive cancers in adults and children. N Engl J Med 2018;378:731–9.
7. Zou HY, Li Q, Engstrom LD, West M, Appleman V, Wong KA, et al. PF-06463922 is a potent and selective next-generation ROS1/ALK inhibitor capable of blocking crizotinib-resistant ROS1 mutations. Proc Natl Acad Sci U S A 2015;112:3493–8.
8. Friboulet L, Li N, Katayama R, Lee CC, Gainor JF, Crystal AS, et al. The ALK inhibitor ceritinib overcomes crizotinib resistance in non-small cell lung cancer. Cancer Discov. 2014;4:662–73.
9. Ou SH, Azada M, Hsiang DJ, Herman JM, Kain TS, Siwak-Tapp C, et al. Next-generation sequencing reveals a Novel NSCLC ALK F1174V mutation and confirms ALK G1202R mutation confers high-level resistance to alectinib (CH5424802/RO5424802) in ALK-rearranged NSCLC patients who progressed on crizotinib. J Thorac Oncol 2014;9:549–53.
10. Gainor JF, Dardaei L, Yoda S, Friboulet L, Leshchiner I, Katayama R, et al. Molecular mechanisms of resistance to first- and second-generation ALK inhibitors in ALK-rearranged lung cancer. Cancer Discov 2016;6:1118–33.
11. Lin JJ, Riely GJ, Shaw AT. Targeting ALK: precision medicine takes on drug resistance. Cancer Discov 2017;7:137–55.
12. Awad MM, Katayama R, McTigue M, Liu W, Deng YL, Brooun A, et al. Acquired resistance to crizotinib from a mutation in CD74-ROS1. N Engl J Med 2013;368:2395–401.
13. Song A, Kim TM, Kim DW, Kim S, Keam B, Lee SH, et al. Molecular changes associated with acquired resistance to crizotinib in ROS1-rearranged non-small cell lung cancer. Clin Cancer Res 2015;21:2379–87.
14. Drilon A, Somwar R, Wagner JP, Vellore NA, Eide CA, Zabriskie MS, et al. A novel crizotinib-resistant solvent-front mutation responsive to cabozantinib therapy in a patient with ROS1-rearranged lung cancer. Clin Cancer Res 2016;22:2351–8.
15. Gainor JF, Tseng D, Yoda S, Dagogo-Jack I, Friboulet L, Lin JJ, et al. Patterns of metastatic spread and mechanisms of resistance to crizotinib in ROS1-positive non-small-cell lung cancer. JCO Precis Oncol 2017;2017. doi: 10.1200/PO.17.00063.
16. Lin JJ, Shaw AT. Recent advances in targeting ROS1 in lung cancer. J Thorac Oncol 2017;12:1611–25.
17. Drilon A, Li G, Dogan S, Gounder M, Shen R, Arcila M, et al. What hides behind the MASC: clinical response and acquired resistance to entrectinib after ETV6-NTRK3 identification in a mammary analogue secretory carcinoma (MASC). Ann Oncol 2016;27:920–6.
18. Russo M, Misale S, Wei G, Siravegna G, Crisafulli G, Lazzari L, et al. Acquired resistance to the TRK inhibitor entrectinib in colorectal cancer. Cancer Discov 2016;6:36–44.
19. Lim SM, Kim HR, Lee JS, Lee KH, Lee YG, Min YJ, et al. Open-Label, Multicenter, phase II study of ceritinib in patients with non-small-cell lung cancer harboring ROS1 rearrangement. J Clin Oncol 2017;35:2613–8.
20. Ahn M-J, Cho BC, Siena S, Drilon A, De Braud F, Krebs MG, et al. Entrectinib in patients with locally advanced or metastatic ROS1 fusion-positive non–small cell lung cancer (NSCLC) rearrangements. Presented at the 18th International Association for the Study of Lung Cancer World Conference on Lung Cancer, Yokohama, Japan, October 15–18, 2017.
21. Katayama R, Kobayashi Y, Friboulet L, Lockerman EL, Koike S, Shaw AT, et al. Cabozantinib overcomes crizotinib resistance in ROS1 fusion-positive cancer. Clin Cancer Res 2015;21:166–74.
22. Shaw AT, Felip E, Bauer TM, Besse B, Navarro A, Postel-Vinay S, et al. Lorlatinib in non-small-cell lung cancer with ALK or ROS1 rearrangement: an international, multicentre, open-label, single-arm first-in-man phase 1 trial. Lancet Oncol 2017;18:1590–9.
23. Solomon BJ, Shaw A, Ou SHI, Besse B, Felip E, Bauer TM, et al. Phase 2 Study of lorlatinib in patients with advanced ALK+/ROS1+ non-small-cell lung cancer. Presented at: the IASLC 18th World Conference on Lung Cancer; October 15–18; Yokohama, Japan. Abstract 8573.
24. Drilon A, Nagasubramanian R, Blake JF, Ku N, Tuch BB, Ebata K, et al. A next-generation TRK kinase inhibitor overcomes acquired resistance to prior TRK kinase inhibition in patients with TRK fusion-positive solid tumors. Cancer Discov 2017;7:963–72.
25. Peters S, Camidge DR, Shaw AT, Gadgeel S, Ahn JS, Kim DW, et al. Alectinib versus crizotinib in untreated ALK-positive non–small-cell lung cancer. N Engl J Med 2017;377:829–38.